Adsorption of Cr(VI) and Cu(II) from aqueous solutions by biochar derived from *Chaenomeles sinensis* seed

Xiaoling Hu, Jianyang Song, Hongyu Wang, Wei Zhang, Bin Wang, Wanlin Lyu, Qilong Wang, Pei Liu, Ling Chen and Jie Xing

ABSTRACT

In order to utilize the discarded *Chaenomeles sinensis* seed (CSS) and develop low-cost biochar for heavy metal pollution control, this study pyrolyzed CSS to prepare biochar at three different temperatures (300, 450 and 600 °C). The physicochemical properties of CSS biochar such as elemental composition, surface area, surface morphology and surface functional groups were characterized. Its adsorption properties including kinetics, isotherms and thermodynamics were studied. The results showed that the adsorption equilibrium was reached at 5 h, which was relatively fast. CSS biochar prepared at 450 °C (CSS450) had the maximum adsorption capacity for Cr(VI) and Cu(II), which was 93.19 mg/g and 105.12 mg/g, respectively. The thermodynamic parameter $\Delta G^0 < 0$ and the isotherm parameter R_L between 0 and 1 all revealed the feasibility and spontaneity of the adsorption process. The removal of Cr(VI) exhibited high efficiency in a wide pH range (1–10), while the removal of Cu(II) was pH-dependent and optimal at pH = 6. The coexisting ions in the solution showed slight inhibition of the adsorption of Cr(VI) and Cu(II). Additionally, Cu(II) exhibited better affinity for CSS450 than Cr(VI) in dynamic adsorption. This is the first study to prepare biochar from CSS and confirms its potential application for heavy metal remediation.

Key words | adsorption, biochar, *Chaenomeles sinensis* seed, copper, hexavalent chromium, waste recycling

Xiaoling Hu
Jianyang Song
Hongyu Wang (corresponding author)
Wei Zhang
Bin Wang
Wanlin Lyu
Qilong Wang
Pei Liu
School of Civil Engineering,
Wuhan University,
Wuhan 430072,
China
E-mail: *hywang96@126.com*

Ling Chen
Department of Internal Medicine & Geriatrics,
Zhongnan Hospital of Wuhan University,
Wuhan 430072,
China

Jie Xing
Hei Longjiang Provincial Research Academy of Environmental Sciences,
Harbin 150056,
China

INTRODUCTION

Chaenomeles sinensis is a deciduous or semi-evergreen tree in the family Rosaceae (Du *et al.* 2013). Its fruit is often used for food and medicinal purposes, and has been used extensively to treat some diseases such as rheumatoid arthritis, hepatitis, asthma and cough (Hamauzu *et al.* 2005; Zhang *et al.* 2010). However, in the process of processing *Chaenomeles sinensis* fruit, its seeds are often discarded (Wang *et al.* 2018), which not only pollutes the environment but also wastes natural resources. In order to make use of the waste, this study tries to use the seeds to produce biochar and solve the increasingly serious environmental problems, so as to make them a low-cost and environmentally friendly source of biochar.

Biochar is a carbon-rich material obtained by pyrolysis of biomass in an oxygen-limited environment (Chen *et al.* 2012). It is widely used in soil remediation and water pollution control to adsorb organic matter and heavy metal ions (Ahmad *et al.* 2014; Zhao *et al.* 2017). In recent years, biomass sources of biochar production have included agricultural crops, plant residues, animal manure and wastewater sludge (Ahmad *et al.* 2014; Wei *et al.* 2019b). Waste biomass has been widely used in biochar production due to its cost and environmental benefits compared with other feedstock (Chen & Chen 2009; Jalayeri & Pepe 2019). The characteristics of biochar are greatly affected by the pyrolysis temperature (Chen *et al.* 2011). The specific surface area, aromatic structural components, porosity and mineral contents of biochar increase with pyrolysis temperature (Li *et al.* 2017; Wei *et al.* 2019a), while the oxygen-containing functional groups, hydrophilicity, polarity and yield decrease (Wang & Wang 2019; Wei *et al.* 2019a; Zhang *et al.* 2019a). The pyrolysis temperature influences the capacity of biochar to adsorb heavy metals by affecting these properties (Wei *et al.* 2019a). Therefore, it is necessary

doi: 10.2166/wst.2020.036

to find suitable conditions to produce biochar with better adsorption performance.

Heavy metals are increasingly becoming common contaminants in the environment and a major concern worldwide due to their properties of non-biodegradability and long-term accumulation (Li *et al.* 2018). Hexavalent chromium is a carcinogen with strong toxicity and oxidization (Zhang *et al.* 2018b). Low doses of copper are essential to humans, but high concentrations of it may be associated with many diseases (Ippolito *et al.* 2012; Jalayeri & Pepe 2019). At present, the methods for the treatment of heavy metal contaminants such as chemical precipitation, ion exchange, reverse osmosis and membrane separation have the shortcomings of high cost and low efficiency when used extensively (Li *et al.* 2017; Ahmad *et al.* 2018). As an adsorbent, biochar is attracting more and more attention in the field of heavy metal treatment due to its characteristics of environmental protection, low cost and simple operation.

Chaenomeles sinensis seed (CSS) is a major residue abundantly generated from *Chaenomeles sinensis* production procedures. Producing biochar by CSS is an effective way of waste recycling and pollutant removal. Extensive studies have been carried out to investigate the remediation of heavy-metal-contaminated water by biochar derived from different waste biomass (Peng *et al.* 2017; Hong *et al.* 2019; Shen *et al.* 2019; Wei *et al.* 2019a). But there is no relevant research about the use of CSS as feedstock to produce biochar. Therefore, this study attempts to directly pyrolyze CSS to produce biochar and to investigate the possibility of its adsorbing heavy metals. The objectives of this study are: (1) to investigate the physicochemical properties of CSS biochars; (2) to evaluate the adsorption performance of CSS biochars for Cr(VI) and Cu(II); (3) to analyze the potential mechanisms of heavy metal adsorption onto CSS biochars.

MATERIALS AND METHODS

Materials

All the reagents used in this work were of analytical grade, and purchased from Sinopharm Chemical Reagent Co., Ltd, China. The solutions were prepared using deionized water. The CSS used in this work were obtained from a beverage factory using *Chaenomeles sinensis* as raw material in Henan province, China.

Production of biochars

The waste was collected from the beverage factory and CSS were picked out. Then they were washed with deionized water and dried in an oven at 80 °C to a constant weight. Then the treated CSS were stored in a desiccator for later use. Biochars were produced by pyrolyzing the treated materials in a tube furnace under N_2 gas conditions for 2 h at 300 °C (CSS300), 450 °C (CSS450) and 600 °C (CSS600), respectively. The three kinds of biochar were ground separately using a mortar, and samples of 0.9–1.0 mm were sieved out and placed in a desiccator for subsequent experiments.

Characterization of biochars

The ash content of the biochars was determined by heating the biochar samples at 800 °C for 4 h (Chen & Chen 2009). The contents of C, H and N in the biochars were measured using an elemental analyzer (RARIO EL III, Elementar, Germany). The content of O was calculated by subtracting the C, H, N and ash contents from the biochar samples (Song *et al.* 2019). The atomic ratios of H/C, O/C, and (N + O)/C were calculated. The yield was calculated by the mass ratio of the obtained biochars to the raw materials. The surface area was measured with N_2 adsorption determined by a multi-channel specific surface area analyzer (TriStar II 3020, Micromeritics, USA) using the Brunauer–Emmett–Teller (BET) method. A scanning electron microscope (SEM, JEM-6700F, Japan) and a Fourier transform infrared spectroscope (FTIR, Thermo Nicolet, 6700, Madison, WI, USA) were used to measure the surface morphology and surface functional groups, respectively.

Adsorption kinetics, isotherms and thermodynamics

For adsorption kinetics, 0.1 g biochar samples were mixed with 50 mL Cr(VI) and Cu(II) solution at an initial concentration of 50 mg/L, respectively. Then the solutions were placed in 250 mL sealed conical bottles and shaken in a shaker at a speed of 120 rpm and temperature of 25 ± 0.5 °C. Samples were taken at intervals of 5, 10, 20, 30, 60, 120, 300, 600, 900, 1,440 and 2,880 minutes. For adsorption isotherms, 0.1 g biochar samples were mixed with 50 mL Cr(VI) and Cu(II) solutions at an initial concentration of 10, 20, 40, 80, 160, 200, 300, 400, 500 mg/L, respectively. The thermodynamics experiments were the same as the kinetics experiments except that they were performed at three different temperatures (25, 35 and 45 °C).

After filtration through 0.45 μm filters, the residual concentration of heavy metal ions in the filtrate was measured by inductively coupled plasma–atomic emission spectrometry (ICP-OES, Optima 4300DV, PerkinElmer SCIEX, USA).

The amounts of heavy metal ions adsorbed per unit of CSS biochar mass at each time point were calculated using the formula:

$$q_t = \frac{(C_0 - C_t)V}{m} \quad (1)$$

where q_t is the adsorption amount at time t (mg/g); C_0 and C_t are the concentrations of heavy metal ions at initial and time t (mg/L), respectively; V is the volume of solution (L); and m is the mass of CSS biochar (g).

In order to study the mechanisms of Cr(VI) and Cu(II) adsorption onto CSS biochars and the rate-controlling step for the adsorption process, as well as the rate at which the target heavy metal ions were adsorbed, the experimental kinetic data were fitted by the following four model equations:

Pseudo-first-order equation: $q_t = q_e(1 - e^{-k_1 t})$ (2)

Pseudo-second-order equation: $q_t = \frac{k_2 q_e^2 t}{1 + k_2 q_e t}$ (3)

Elovich equation: $q_t = \frac{1}{\beta}\ln(1 + \alpha\beta t)$ (4)

Intra-particle diffusion equation: $q_t = K_{3,i} t^{\frac{1}{2}} + C_i$ (5)

where q_e is the adsorption amount at equilibrium (mg/g); k_1 and k_2 are the first-order adsorption rate constant and the second-order adsorption rate constant (h^{-1}), respectively; $K_{3,i}$ is the intra-particle diffusion rate constant [mg/(g·min$^{1/2}$)]; α and β are the initial adsorption rate constant (mg/kg) and the desorption constant (kg/mg), respectively; and C_i is the intercept representing the thickness of the boundary layer.

The adsorption isotherm data were fitted by two typical isotherm models (Langmuir and Freundlich). The equations of the two models were as follows:

Langmuir equation: $q_e = \frac{K S_{max} C_e}{1 + K C_e}$ (6)

Freundlich equation: $q_e = K_f C_e^n$ (7)

where S_{max} is the maximum adsorption capacity (mg/g); C_e is the sorbate concentration in solutions under equilibrium conditions (mg/L); K and K_f are the Langmuir bonding term related to interaction energies (L/mg) and the Freundlich affinity coefficient (mg$^{(1-n)}$ L^n/g), respectively; and n is the Freundlich linearity constant.

Thermodynamic parameters including free energy (ΔG^0), enthalpy (ΔH^0) and entropy (ΔS^0) could be calculated using the following formulae (Li *et al.* 2018):

$$\ln K^0 = \frac{\Delta S^0}{R} - \frac{\Delta H^0}{RT} \quad (8)$$

$$\Delta G^0 = -RT \ln K^0 \quad (9)$$

$$K^0 = \frac{a q_e}{C_e} \quad (10)$$

where K^0 is the equilibrium constant; R is the universal gas constant [8.314 J/(mol·K)]; T is the absolute temperature in Kelvin (K); and a is the adsorbent dose (g/L).

Effects of pH and ionic strength

The initial concentrations of Cr(VI) and Cu(II) solutions were set to 100 mg/L. The initial pH of Cr(VI) and Cu(II) solutions varied between 1–10 and 1–7, respectively. And the NaCl concentration varied between 0 and 0.5 mol/L. Other experimental conditions were the same as that in the preceding subsection.

Dynamic sorption experiments

Biochar samples of 3 g were filled into a glass column with the specification of $D \times H = 16\ \text{mm} \times 240\ \text{mm}$. A peristaltic pump was used to make the mixed solution with Cr(VI) and Cu(II) concentrations both of 100 mg/L flow through the CSS biochars from bottom to top of the glass column at a flow rate of 20 mL/h. The samples were collected at the top of the adsorption column and the concentration of Cr(VI) and Cu(II) ions remaining was examined to investigate the efficiency and prioritization of Cr(VI) and Cu(II) ions during dynamic adsorption.

RESULTS AND DISCUSSION

Characterization of biochar

The physicochemical properties of biochars produced at different pyrolysis temperatures are shown in Table 1. As shown, the yields of the three biochars were in the range of 25.04–59.94% and negatively correlated with pyrolysis

Table 1 | Yields, elemental compositions, atomic ratios, ash contents and BET surface area of the CSS biochars

Biochar	Yield (%)	C	H	N	O	(N + O)/C	O/C	H/C	Ash	BET surface area (m^2/g)
CSS300	59.94	70.30	6.82	3.36	18.13	0.306	0.258	0.097	1.38	0.61
CSS450	26.87	67.82	3.11	4.34	11.68	0.236	0.172	0.046	13.05	3.24
CSS600	25.04	71.63	2.33	3.93	6.76	0.149	0.094	0.033	15.35	80.55

temperature (300–600 °C), which was consistent with previous literature (Uchimiya *et al.* 2011; Zhao *et al.* 2018). In addition, the pyrolysis temperature had significant effects on the elemental compositions and ash contents of the biochars. Specifically, the increasing of pyrolysis temperature caused an increase in the C content and decreases in the H and O contents. As the temperature rose from 300 °C to 600 °C, the C content fluctuated between 67.82% and 71.63%, and the contents of H and O decreased from 6.82% to 2.33% and 18.13% to 6.76%, respectively. These might be due to an increase in the degree of carbonization of plant-derived biochar at higher temperatures (Wei *et al.* 2019b), the reduction of volatiles, and the destruction of surface hydroxyl groups and H and O atoms in combination with C in biochar (Novak *et al.* 2009). Temperature had no significant effect on the change of N content (Ahmad *et al.* 2014). This resulted in lower H/C and O/C ratios, and (N + O)/C also decreased. These indicated that the aromaticity of the biochars was enhanced and the polarity reduced. The ash contents increased with the pyrolysis temperature. Especially when the pyrolysis temperature was raised from 300 °C to 450 °C, the ash contents were greatly increased. The ash was mainly inorganic salts in CSS. The increasing of pyrolysis temperature led to the loss of volatile organic compounds and other organic matter, and thus the relative content of ash in the biochars increased.

Table 1 also shows that the BET surface area of CSS450 (3.24 m^2/g) was about five times larger than that of CSS300 (0.61 m^2/g). As the pyrolysis temperature rose to 600 °C, the BET surface area of CSS600 (80.55 m^2/g) increased markedly. Many amorphous carbons remained in the biochars at lower temperatures and hindered the formation of pores, so the biochars produced at lower temperatures had a small BET surface area. As the temperature increased, the gas released by the destruction of the unstable volatile components thus produced many pore structures, causing an increase in the BET surface area (Kumar *et al.* 2017).

Figure 1 shows the morphologies of the three biochars. As can be seen, the surface of CSS300 was smooth and had irregular protrusions, but no shaped pores were visible. When the pyrolysis temperature rose to 450 °C, pores having a diameter of about 10 μm with a thickness interval of about 4 μm were formed. The surface of CSS600 had a large number of dense pores, and micropores could be observed on it. This further demonstrated an increase in the BET surface area, which could provide a larger contact area and more adsorption sites for heavy metals.

The FTIR spectra of CSS biochars are presented in Figure 2. As the pyrolysis temperature increased, the functional groups on the surface of the biochars were significantly reduced, especially when the pyrolysis temperature rose from 300 °C to 450 °C. The stretching vibration of alcoholic and phenolic –OH occurred at 3,459 cm^{-1}. The vibration of aliphatic C–H occurred at 2,929 cm^{-1}. The skeleton vibration at 1,589 cm^{-1} was attributed to C = C and C = O in aromatic rings of conjugated ketones and quinines. The stretching vibration of –COOH occurred at 1,396 cm^{-1}, and the stretching vibration at 1,106 cm^{-1} was attributed to C–O–C in cellulose and hemicellulose (Chen & Chen 2009; Tong *et al.* 2011; Zhang *et al.* 2018a; Chen *et al.* 2019). The variations of peak intensity reflected the gradual condensation of aromatic structures and the gradual decomposition of lignin, hemicellulose and cellulose with the increase of temperature (Keiluweit *et al.* 2010). The presence of a large number of oxygen-containing functional groups in the CSS biochars provided the possibility of adsorbing heavy metals.

Adsorption kinetics, isotherms and thermodynamics

It was clear that both the adsorption process of Cr(VI) and Cu(II) by CSS biochars could be divided into an initial rapid adsorption phase and a slow phase after equilibrium (Figure 3(a) and 3(c)) (Wang *et al.* 2015). It was found that CSS450 had the maximum adsorption capacity for Cr(VI) and Cu(II). The adsorption capacity of Cr(VI) on CSS450 was 15.04 mg/g at 1 h, and 18.61 mg/g at equilibrium. The adsorption capacity of Cu(II) on CSS450 was 13.76 mg/g at 2 h, and 15.78 mg/g at the final equilibrium phase. It can also be seen that adsorption equilibrium was almost reached at 5 h and complete adsorption was achieved,

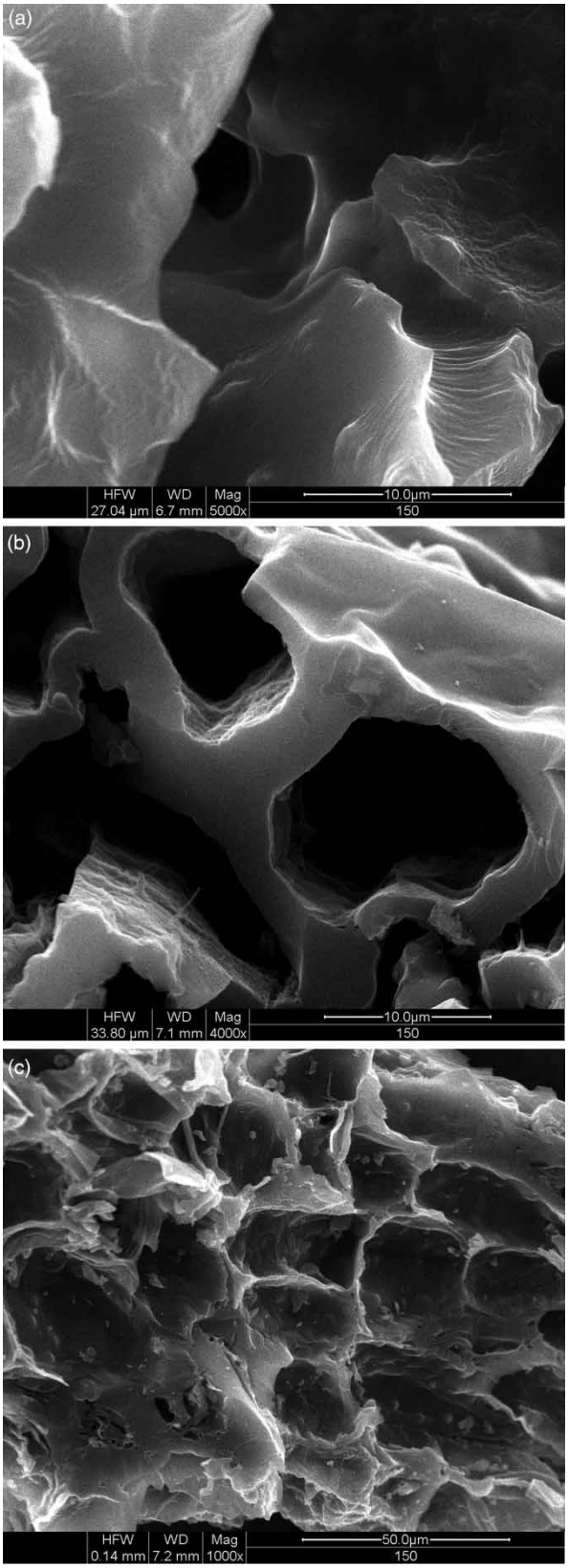

Figure 1 | The SEM images of (a) CSS300, (b) CSS450 and (c) CSS600.

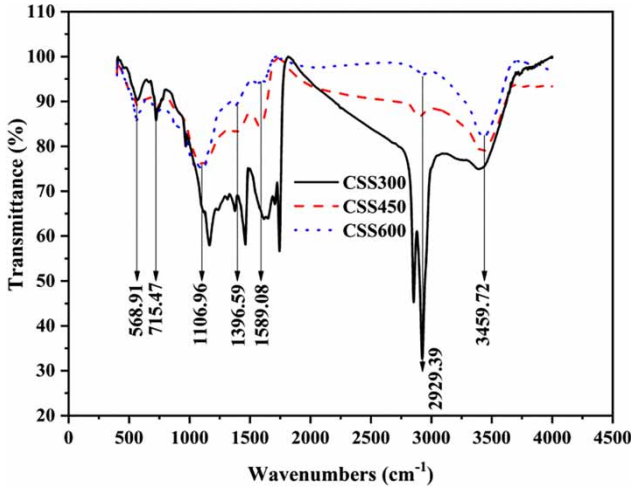

Figure 2 | FTIR spectra of CSS300, CSS450 and CSS600.

which was faster than that in some previous studies (Tytłak *et al.* 2015; Jalayeri & Pepe 2019).

The fitting results of the pseudo-first-order, pseudo-second-order and Elovich equations for the kinetic experimental data are shown in Figure 3 and Table 2. The correlation coefficients of the pseudo-second-order model for the adsorption of Cr(VI) and Cu(II) on the CSS biochars were both $R^2 > 0.98$, which were higher than the other two models. And the equilibrium adsorption amounts q_e calculated by the pseudo-second-order model were also close to the experimental data. This suggests that the adsorption process of Cr(VI) and Cu(II) on the CSS biochars was controlled by a chemical adsorption mechanism, and the adsorption rate was related to the adsorption sites on the adsorbent surface (Li *et al.* 2018; Zhang *et al.* 2019b). It could also be found that the increase of pyrolysis temperature was not conducive to the adsorption of Cr(VI) and Cu(II) on CSS biochars, which might be due to the destruction of functional groups on the surface of the biochars at high temperatures and that was detrimental to the chemical interaction of heavy metal ions with biochars. At the same time, the adsorption performance of Cr(VI) and Cu(II) by CSS biochars was not ideal when the pyrolysis temperature was 300 °C. This might be because the temperature was too low to generate enough pores to provide sufficient contact area.

The intra-particle diffusion models of Cr(VI) and Cu(II) are shown in Figure 3(b) and 3(d), respectively. Neither for Cr(VI) nor for Cu(II) did the linear portions pass through the origin. This indicates that intra-particle diffusion was not the only rate-controlling step, and the adsorption of Cr(VI) and Cu(II) onto the CSS biochars was controlled by more than one process (Shakya & Agarwal 2019). The

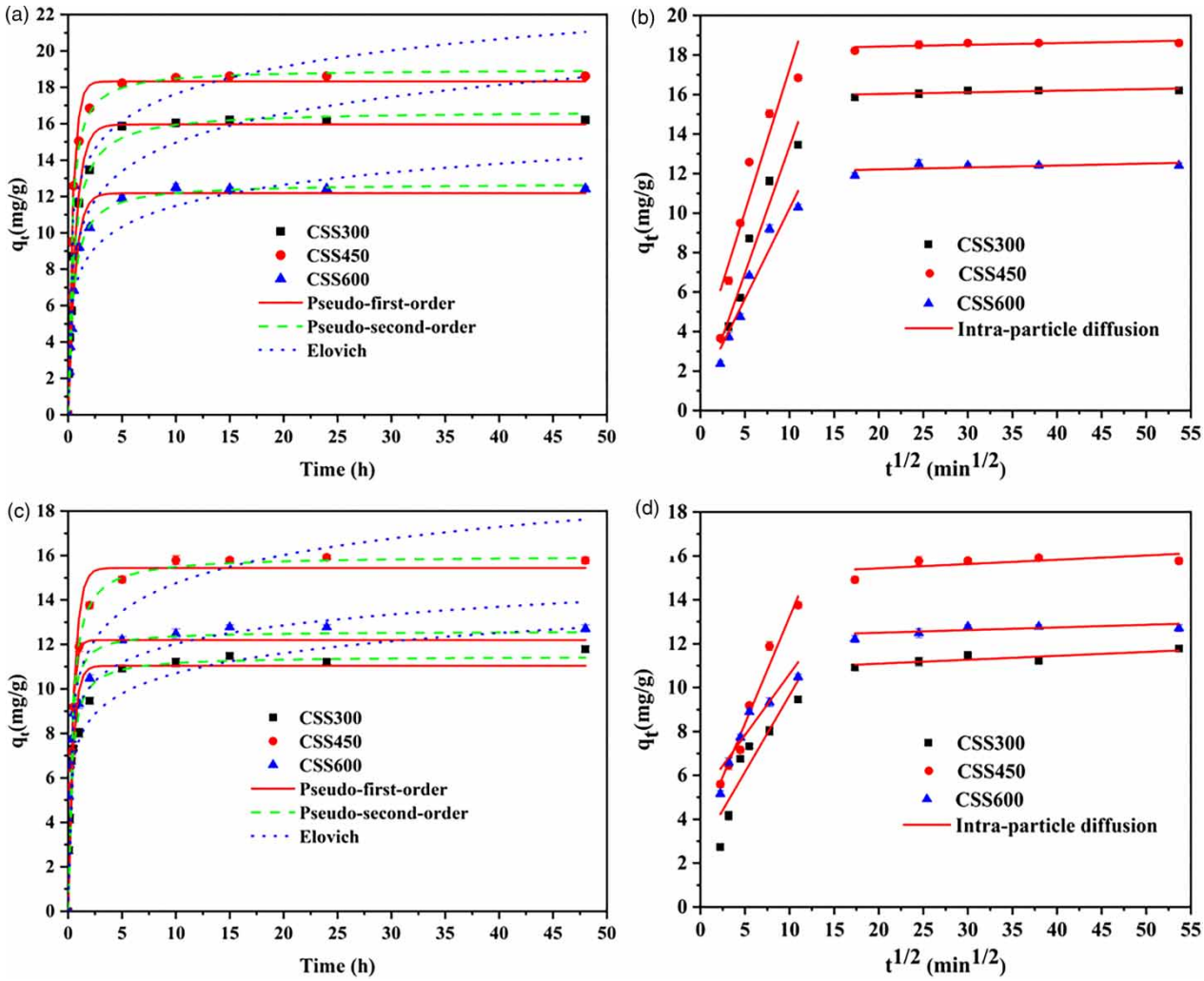

Figure 3 | The pseudo-first-order, the pseudo-second-order and Elovich equations of (a) Cr(VI) and (c) Cu(II) and the intra-particle diffusion model of (b) Cr(VI) and (d) Cu(II).

adsorption process of Cr(VI) and Cu(II) onto the CSS biochars mainly consisted of two stages: the initial linear portion related to surface diffusion and the latter linear portion related to pore diffusion (Venugopal & Mohanty 2011). As shown in Table 2, the larger rate constant $K_{3,1}$ corresponds to a fast diffusion process of Cr(VI) and Cu(II) from the liquid to the surface of the CSS biochar. The smaller rate constant $K_{3,2}$ in the second stage indicates that intraparticle diffusion was relatively slow and gradually reached equilibrium. The increasing values of the boundary layer constants C_i indicate the greater boundary effect of the adsorption of Cr(VI) and Cu(II) onto the CSS biochars.

Adsorption isotherms and models play an important role in understanding the adsorption mechanism. Models such as Langmuir, Freundlich, Dubinin–Radushkevich, Temkin and some statistical physics models have been used to simulate the adsorption isotherms (Dotto *et al.* 2015; Sellaoui *et al.* 2015; Niazi *et al.* 2018). In this study, the adsorption isotherm experimental data were investigated by two very common models (Langmuir and Freundlich) and the fitting results of Cr(VI) and Cu(II) adsorption onto CSS biochars are shown in Figure 4 and Table 3. The adsorption amounts of Cr(VI) and Cu(II) on the CSS biochars were gradually increased as the concentrations of Cr(VI) and Cu(II) increased from 0 to 500 mg/L. When the concentration of heavy metal ions was small, the adsorption sites on the surface of the biochars were sufficient to react with heavy metals quickly. When the concentration continued to increase, the number of available adsorption sites was limited. The adsorption capacity order of Cr(VI) and Cu(II) adsorbed by CSS biochars produced at different pyrolysis temperatures was CSS450 > CSS600 > CSS300.

Table 2 | Kinetic parameters of Cr(VI) and Cu(II) adsorption by CSS biochars

Adsorbate	Biochar	Kinetics models	Parameter-1	Parameter-2	R^2
Cr(VI)	CSS300	Pseudo-first-order	$k_1 = 1.4538 \pm 0.0952$	$q_e = 15.9624 \pm 0.2421$	0.9919
		Pseudo-second-order	$k_2 = 0.1213 \pm 0.0079$	$q_e = 16.7232 \pm 0.1853$	0.9964
		Elovich	$\alpha = 158.4268 \pm 87.6556$	$\beta = 0.4372 \pm 0.0495$	0.9462
		Intra-particle diffusion	$K_{3,1} = 1.2824 \pm 0.1883$	$C_1 = 0.5688 \pm 1.1838$	0.9206
			$K_{3,2} = 0.0082 \pm 0.0048$	$C_2 = 15.8648 \pm 0.1688$	0.4967
	CSS450	Pseudo-first-order	$k_1 = 2.2667 \pm 0.1197$	$q_e = 18.3229 \pm 0.2212$	0.9941
		Pseudo-second-order	$k_2 = 0.1825 \pm 0.0103$	$q_e = 19.0092 \pm 0.1686$	0.9972
		Elovich	$\alpha = 732.2588 \pm 622.8323$	$\beta = 0.4606 \pm 0.0625$	0.9336
		Intra-particle diffusion	$K_{3,1} = 1.4445 \pm 0.3052$	$C_1 = 2.8679 \pm 1.9182$	0.8485
			$K_{3,2} = 0.0087 \pm 0.0054$	$C_2 = 18.2596 \pm 0.1914$	0.4593
	CSS600	Pseudo-first-order	$k_1 = 1.5822 \pm 0.1246$	$q_e = 12.1774 \pm 0.2228$	0.9877
		Pseudo-second-order	$k_2 = 0.1771 \pm 0.0105$	$q_e = 12.7298 \pm 0.1268$	0.9969
		Elovich	$\alpha = 163.2056 \pm 88.1087$	$\beta = 0.5995 \pm 0.0625$	0.9546
		Intra-particle diffusion	$K_{3,1} = 0.9150 \pm 0.1310$	$C_1 = 1.1000 \pm 0.5270$	0.9235
			$K_{3,2} = 0.0099 \pm 0.0080$	$C_2 = 12.0103 \pm 0.2827$	0.3384
Cu(II)	CSS300	Pseudo-first-order	$k_1 = 2.3162 \pm 0.2708$	$q_e = 11.0375 \pm 0.2946$	0.9708
		Pseudo-second-order	$k_2 = 0.3081 \pm 0.0254$	$q_e = 11.4778 \pm 0.1479$	0.9941
		Elovich	$\alpha = 460.5486 \pm 292.4894$	$\beta = 0.7630 \pm 0.0769$	0.9626
		Intra-particle diffusion	$K_{3,1} = 0.6992 \pm 0.1744$	$C_1 = 2.6729 \pm 1.0967$	0.8006
			$K_{3,2} = 0.0179 \pm 0.0096$	$C_2 = 10.7332 \pm 0.3385$	0.5375
	CSS450	Pseudo-first-order	$k_1 = 1.9490 \pm 0.2604$	$q_e = 15.4417 \pm 0.4785$	0.9603
		Pseudo-second-order	$k_2 = 0.1922 \pm 0.0260$	$q_e = 15.9951 \pm 0.3466$	0.9831
		Elovich	$\alpha = 586.6551 \pm 330.5864$	$\beta = 0.5472 \pm 0.0496$	0.9691
		Intra-particle diffusion	$K_{3,1} = 0.9725 \pm 0.0845$	$C_1 = 3.5128 \pm 0.5312$	0.9707
			$K_{3,2} = 0.0195 \pm 0.0138$	$C_2 = 15.0474 \pm 0.4856$	0.4015
	CSS600	Pseudo-first-order	$k_1 = 3.0935 \pm 0.5221$	$q_e = 12.1968 \pm 0.4399$	0.9406
		Pseudo-second-order	$k_2 = 0.4259 \pm 0.0612$	$q_e = 12.5965 \pm 0.2566$	0.9829
		Elovich	$\alpha = 2{,}579.3351 \pm 1{,}657.3766$	$\beta = 0.8293 \pm 0.0666$	0.9815
		Intra-particle diffusion	$K_{3,1} = 0.5578 \pm 0.1302$	$C_1 = 5.0515 \pm 0.8181$	0.8212
			$K_{3,2} = 0.0120 \pm 0.0085$	$C_2 = 12.26334 \pm 0.3012$	0.3970

The results were consistent with the adsorption kinetics that CSS450 had the largest adsorption capacity for Cr(VI) and Cu(II).

For the adsorption of Cr(VI) onto the CSS biochars, the Langmuir model was more suitable for describing it with $R^2 > 0.9909$. It indicated that the adsorption of Cr(VI) was monolayer adsorption. After a certain number of adsorption sites on the surface of the CSS biochars were occupied by Cr(VI) ions, ions could not be accepted again (Zhou *et al.* 2016). For the adsorption of Cu(II) on the CSS biochars, the correlation coefficient fitted by the Freundlich model was higher than that of the Langmuir with $R^2 = 0.9752$–0.9938, reflecting that the Freundlich model was more suitable for describing it. It indicated that the adsorption of Cu(II) onto the CSS biochars was chemical adsorption on a heterogeneous surface, which might have a greater relationship with the functional groups on the surface of the CSS biochars and the interaction between adsorbent and adsorbate (Deng *et al.* 2009).

Based on the Langmuir model, the feasibility of adsorption was further explored using the dimensionless separation factor R_L ($R_L = 1/(1 + KC_0)$). The values of R_L between 0 and 1 indicated the feasibility of the adsorption process (Kołodyńska *et al.* 2012). As shown in Table 3, the values of R_L were all within the range of 0–1, indicating the favorability of Cr(VI) and Cu(II) adsorption onto the CSS biochars. Furthermore, the values of R_L of Cu(II) adsorption onto CSS450 were lower than those of Cr(VI), which corresponded to a higher affinity between Cu(II) and CSS450.

According to the fitting results, the calculated maximum adsorption capacities S_{max} of CSS450 for Cr(VI) and Cu(II) were 93.19 mg/g and 105.12 mg/g, respectively, which were higher than those of direct pyrolytic biochars or the biochars obtained by some modification methods reported in many other studies (Table 4). It indicated that the biochars obtained by pyrolyzing CSS directly had great potential as a cost-effective adsorbent for treating heavy metal contamination in the environment.

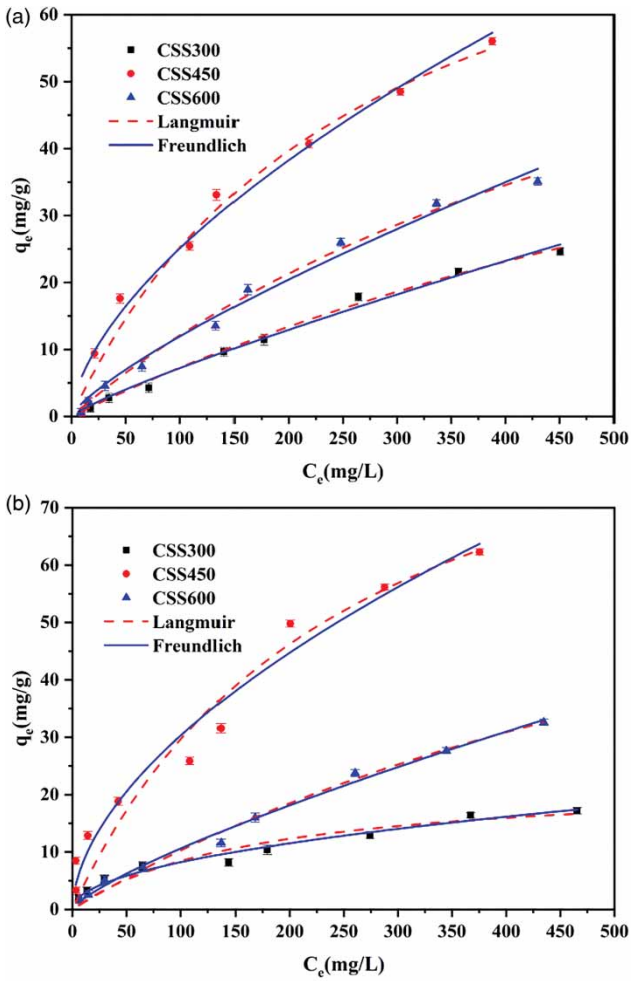

Figure 4 | Sorption isotherm data and fitted models of (a) Cr(VI) and (b) Cu(II) onto CSS biochars.

The thermodynamic studies on the adsorption of Cr(VI) and Cu(II) onto CSS biochars are shown in Figure 5 and Table 5. Obviously, the equilibrium constant K^0 increased with the temperature in the range of temperature studied, indicating that the higher temperature strengthened the adsorption process. A negative value of ΔG^0 shows that the adsorption of Cr(VI) and Cu(II) onto the CSS biochars was feasible and spontaneous. In addition, the value of ΔG^0 was reduced with temperature increase which mainly reflects the greater drive force and higher adsorption capacity (Zhang *et al.* 2019b). The positive values of ΔH^0 and ΔS^0 indicate that all the adsorption process was endothermic and the randomness at the solid–liquid interface increased, respectively (Li *et al.* 2018). At the same temperature, the minimum values of ΔG^0 of the adsorption of Cr(VI) and Cu(II) onto CSS450 revealed better spontaneity than the other two kinds of biochar, and further corresponded to the better adsorption performance of CSS450. The values of ΔH^0 of Cr(VI) (25.6714 kJ/mol) and Cu(II) (29.2075 kJ/mol) adsorption onto CSS450 indicated the existence of chemisorption (Zhang *et al.* 2018b).

As mentioned above, CSS450 had sufficient surface area, a certain number of surface functional groups and the largest adsorption capacities for Cr(VI) and Cu(II). And the adsorption process showed a better spontaneity. Thus CSS450 was selected for the further adsorption test.

Effects of pH and ionic strength

The pH had significant effects on the adsorption of Cr(VI) and Cu(II) by CSS450 in aqueous solution, which was mainly due to the speciation of metal ions and the charge on the surface of biochars depending on the pH values. The maximum adsorption amounts of Cr(VI) by CSS450 occurred at pH 1 and decreased significantly during the increase of pH from 1 to 2. As the pH continued to rise to

Table 3 | Isotherm parameters of Cr(VI) and Cu(II) adsorption by CSS biochars

Adsorbate	Biochar	Isotherm models	Parameter-1	Parameter-2	R_L	R^2
Cr(VI)	CSS300	Langmuir	$K = 0.0009 \pm 0.0003$	$S_{max} = 84.54 \pm 17.01$	0.6897–0.9911	0.9956
		Freundlich	$K_f = 0.1477 \pm 0.0453$	$n = 0.8442 \pm 0.0525$		0.9914
	CSS450	Langmuir	$K = 0.0037 \pm 0.0009$	$S_{max} = 93.19 \pm 11.89$	0.3509–0.9643	0.9909
		Freundlich	$K_f = 1.5148 \pm 0.0665$	$n = 0.6095 \pm 0.0079$		0.9854
	CSS600	Langmuir	$K = 0.0015 \pm 0.0003$	$S_{max} = 90.76 \pm 13.69$	0.5714–0.9852	0.9944
		Freundlich	$K_f = 0.3367 \pm 0.1058$	$n = 0.7749 \pm 0.0544$		0.9885
Cu(II)	CSS300	Langmuir	$K = 0.0059 \pm 0.0024$	$S_{max} = 22.69 \pm 3.44$	0.2532–0.9443	0.9331
		Freundlich	$K_f = 0.8711 \pm 0.1903$	$n = 0.4874 \pm 0.0382$		0.9801
	CSS450	Langmuir	$K = 0.0039 \pm 0.0016$	$S_{max} = 105.12 \pm 22.08$	0.3390–0.9625	0.9583
		Freundlich	$K_f = 2.2767 \pm 0.7242$	$n = 0.5621 \pm 0.0572$		0.9752
	CSS600	Langmuir	$K = 0.0012 \pm 0.0004$	$S_{max} = 93.42 \pm 19.85$	0.6250–0.9881	0.9921
		Freundlich	$K_f = 0.3028 \pm 0.0697$	$n = 0.7723 \pm 0.0397$		0.9938

Table 4 | Comparison of maximum adsorption capacities of biochars in the literature

Adsorbate	Adsorbent	Adsorption capacity (mg/g)	Reference
Cr(VI)	Modified *Enteromorpha prolifera* biochar	91.5	Chen *et al.* (2018)
	Modified corn stover biochar	24.5	Li *et al.* (2018)
	Coconut coir biochar	31.1	Shen *et al.* (2012)
	Ramie biochar	82.23	Zhou *et al.* (2016)
	Wheat straw biochar	24.6	Tytłak *et al.* (2015)
	Chaenomeles sinensis seed biochar	93.19	This study
Cu(II)	Modified corn stover biochar	91.2	Li *et al.* (2018)
	Corn straw biochar	12.52	Chen *et al.* (2011)
	Hardwood biochar	6.79	Chen *et al.* (2011)
	Pistachio green hull biochar	19.84	Jalayeri & Pepe (2019)
	Cauliflower leaves biochar	53.96	Ahmad *et al.* (2018)
	Chaenomeles sinensis seed biochar	105.12	This study

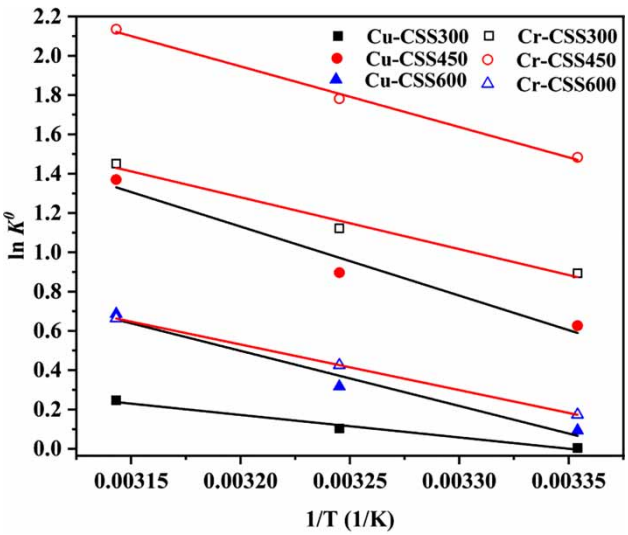

Figure 5 | The van 't Hoff plot for the adsorption of Cr(VI) and Cu(II) onto CSS biochars.

10, the adsorption amounts showed a slight decrease but tended to be stable (Figure 6(a)). In general, Cr(VI) could be effectively removed in a wide pH range (1–10), indicating that CSS450 could be applied in wider pH conditions compared with pineapple peel biochar (Shakya & Agarwal 2019).

It has been reported that electrostatic attraction and complexation are the two main mechanisms by which biochars adsorb Cr(VI) in aqueous solution (Li *et al.* 2017). At pH <6.0, Cr(VI) existed mainly in the form of $Cr_2O_7^{2-}$ and $HCrO_4^-$ (Richard & Bourg 1991). The functional groups on the surface of the biochars were protonated and positively charged under low pH conditions, which was beneficial to electrostatic attraction with negatively charged chromium. When pH >6.0, CrO_4^{2-} was the main form of Cr(VI) (Richard & Bourg 1991), and the deprotonation of the functional groups on the surface of the biochars was not conducive to electrostatic attraction with negatively charged chromium, which hindered further complexation.

The adsorption amounts of Cu(II) onto CSS450 increased from 2.96 mg/g at pH = 1 to 41.45 mg/g at pH = 7 (Figure 6(b)). This was consistent with previous reports that the adsorption of copper onto biochars was pH-dependent (Ippolito *et al.* 2012). Most of the copper was present in its free ionic form (Cu^{2+}) (Chen *et al.* 2011), and partially hydrolyzed to form $Cu(OH)^+$ as the solution pH increased (Tong *et al.* 2011). Because the electronegativity of CSS450 increased with pH, electrostatic attraction between biochars and copper ions was enhanced. The organic functional groups on the surface of CSS450 were dissociated with rising pH, making it easier to combine with Cu^{2+} to form surface complexes. And at higher pH conditions, the affinity of the adsorbent surface for $Cu(OH)^+$ increased (Tong *et al.* 2011). These all led to a higher adsorption capacity for Cu(II) by CSS450 at higher pH conditions.

As shown in Figure 7, the coexisting ion Na^+ in the solution caused a slight inhibition in the adsorption of Cr(VI) and Cu(II) by CSS450, and the inhibition increased with the Na^+ concentration. The same positively charged Na^+ would compete with heavy metal ions for adsorption sites on the surface of the biochars, while the number of adsorption sites was limited. The increase of Na^+ concentration made the competition more intense, and the adsorption sites that could bind to heavy metal ions decreased, resulting in a decrease in the adsorption of Cr(VI) and Cu(II). Moreover, sodium ions might exchange heavy metal ions that had been adsorbed (Liu *et al.* 2014; Wang *et al.* 2015), which was one of the possible reasons for the decrease in adsorption amounts.

Table 5 | Thermodynamic parameters of Cr(VI) and Cu(II) adsorption by CSS biochars

Adsorbate	Biochar	Temperature (°C)	lnK^0	ΔG^0 (kJ/mol)	ΔH^0 (kJ/mol)	ΔS^0 [J/(mol·K)]
Cr(VI)	CSS300	25	0.8932	−2.2140	21.9379	80.8451
		35	1.1211	−2.8722		
		45	1.4508	−3.8376		
	CSS450	25	1.4833	−3.6769	25.6714	98.3309
		35	1.7811	−4.5631		
		45	2.1352	−5.6478		
	CSS600	25	0.1740	−0.4312	18.5637	66.2149
		35	0.4253	−1.0896		
		45	0.6638	−1.7557		
Cu(II)	CSS300	25	0.0045	−0.0112	9.5349	31.9469
		35	0.1032	−0.2645		
		45	0.2469	−0.6530		
	CSS450	25	0.6269	−1.5540	29.2075	102.8695
		35	0.8968	−2.2975		
		45	1.3701	−3.6240		
	CSS600	25	0.0935	−0.2318	23.3257	78.7905
		35	0.3171	−0.8124		
		45	0.6869	−1.8168		

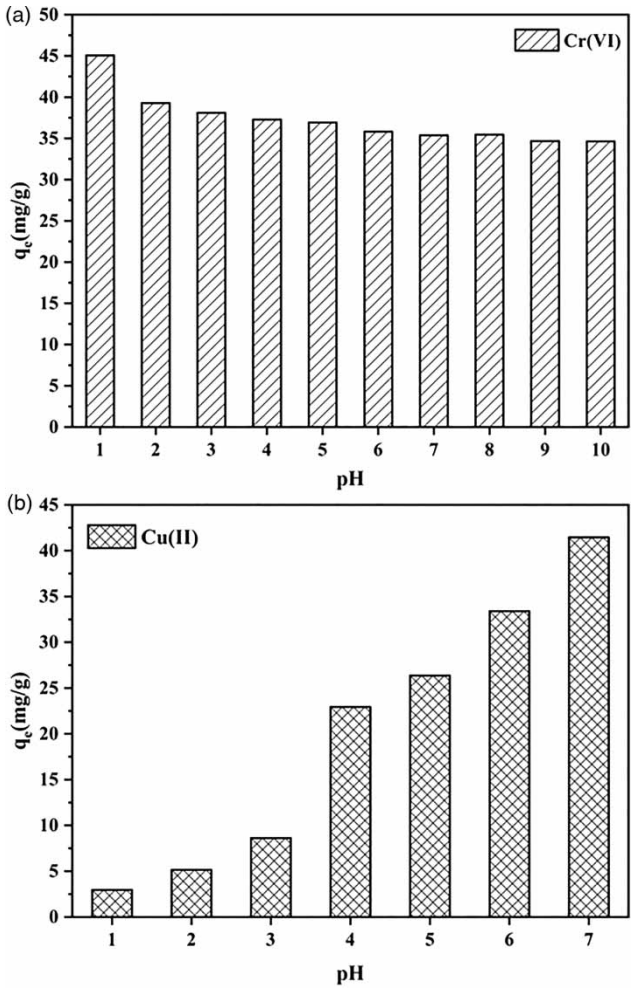

Figure 6 | Effects of initial pH on (a) Cr(VI) and (b) Cu(II) adsorption onto CSS450.

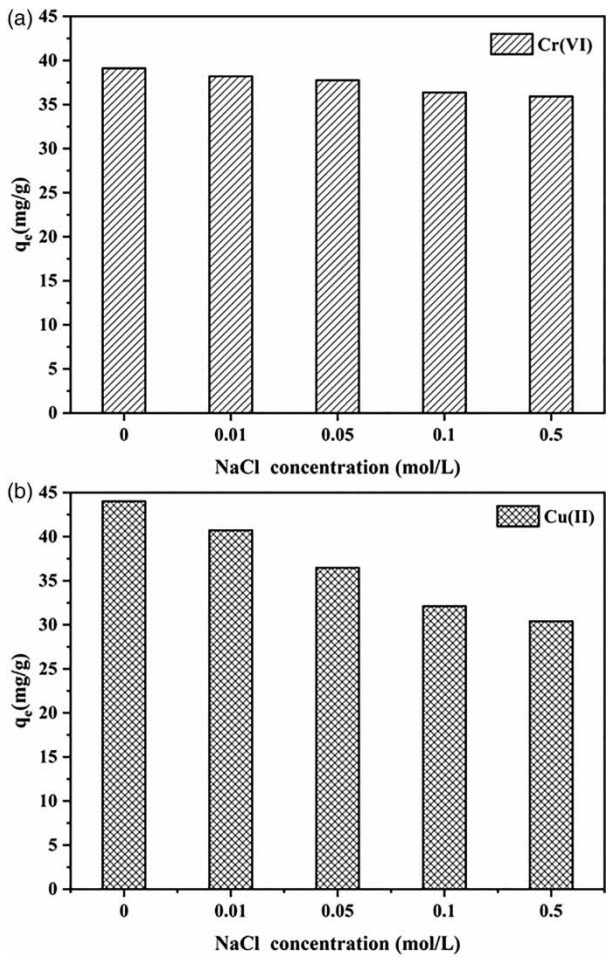

Figure 7 | Effects of solution ionic strength on (a) Cr(VI) and (b) Cu(II) adsorption onto CSS450.

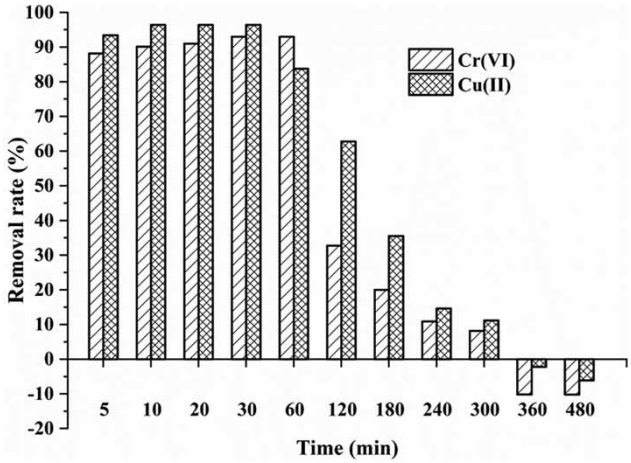

Figure 8 | Dynamic adsorption experiments of Cr(VI) and Cu(II) onto CSS450.

Dynamic sorption experiments

In the first five minutes, the removal of Cr(VI) and Cu(II) reached 88.2% and 93.4%, respectively, and peaked at 30 min (Figure 8). At the beginning of the reaction, there were excessive adsorption sites on the surface of CSS450, so Cr(VI) and Cu(II) could be rapidly adsorbed onto different adsorption sites. Then the removal rates and the adsorption amounts decreased due to the limited adsorption sites on the surface of CSS450. And there might be competition between the two ions (Yang *et al.* 2016; Han *et al.* 2017; Ji & Pei 2019). Desorption occurred at 6 h, but the phenomenon was not greatly aggravated at 8 h. This indicated that the adsorption sites on the surface of CSS450 were saturated and could no longer be combined with heavy metal ions. A small amount of desorption showed that the combination of Cr(VI) and Cu(II) onto CSS450 was stable. During the dynamic adsorption test, Cu(II) showed a better affinity for CSS450 compared with Cr(VI). This finding was in harmony with the adsorption isotherm results and previous research (Song *et al.* 2019).

Sorption mechanisms

Although the surface area of the CSS biochars increased with pyrolysis temperature, the adsorption capacities of heavy metal ions decreased, because the surface oxygen-containing functional groups were lost as the pyrolysis temperature increased. It was obvious that the adsorption of heavy metal ions onto the CSS biochars was associated with oxygen-containing functional groups which could combine with heavy metal ions through a complexation mechanism. There was an initial rapid adsorption phase in the adsorption kinetics, and it could be seen from the FTIR spectrum that CSS300 had the largest number of functional groups, but sufficient pores had not been formed to provide space for heavy metal ions, indicating the existence of physical adsorption. The effects of pH on the adsorption indicated that electrostatic attraction was also one of the main mechanisms for CSS biochars adsorbing heavy metal ions.

CONCLUSIONS

The physicochemical properties of CSS biochar produced at different temperatures and its adsorption performance for Cr(VI) and Cu(II) removal were investigated. The increase in the pyrolysis temperature resulted in an increase in the surface area and a decrease in surface functional groups of the CSS biochar. Adsorption processes of Cr(VI) were strongly correlated with the pseudo-second-order kinetic model and the Langmuir isotherm model, while the adsorption of Cu(II) correlated with the pseudo-second-order kinetic model and Freundlich isotherm model. Thermodynamic studies revealed the feasibility and spontaneity of the adsorption process. Moreover, it exhibited highly efficient Cr(VI) removal in a wide pH range (1–10), while it possessed pH-dependent Cu(II) adsorption characteristics optimal at pH = 6. Crucially, ionic strength could slightly affect the adsorption performance. Results also indicated that the mechanism of Cr(VI) and Cu(II) sorption by CSS biochar is a combination of chemical adsorption and physical adsorption. This study confirmed the potential of CSS as feedstock to prepare low-cost and high-efficiency biochar.

ACKNOWLEDGEMENTS

This work was financially supported by the CRSRI Open Research Program (SN: CKWV2016399/KY).

REFERENCES

Ahmad, M., Rajapaksha, A. U., Lim, J. E., Zhang, M., Bolan, N., Mohan, D., Vithanage, M., Lee, S. S. & Ok, Y. S. 2014 Biochar as a sorbent for contaminant management in soil and water: a review. *Chemosphere* **99**, 19–33.

Ahmad, Z., Gao, B., Mosa, A., Yu, H., Yin, X., Bashir, A., Ghoveisi, H. & Wang, S. 2018 Removal of Cu(II), Cd(II) and Pb(II) ions from aqueous solutions by biochars derived from

potassium-rich biomass. *Journal of Cleaner Production* **180**, 437–449.

Chen, B. & Chen, Z. 2009 Sorption of naphthalene and 1-naphthol by biochars of orange peels with different pyrolytic temperatures. *Chemosphere* **76** (1), 127–133.

Chen, X., Chen, G., Chen, L., Chen, Y., Lehmann, J., McBride, M. B. & Hay, A. G. 2011 Adsorption of copper and zinc by biochars produced from pyrolysis of hardwood and corn straw in aqueous solution. *Bioresource Technology* **102** (19), 8877–8884.

Chen, Z., Chen, B. & Chiou, C. T. 2012 Fast and slow rates of naphthalene sorption to biochars produced at different temperatures. *Environmental Science & Technology* **46** (20), 11104–11111.

Chen, Y., Wang, B., Xin, J., Sun, P. & Wu, D. 2018 Adsorption behavior and mechanism of Cr(VI) by modified biochar derived from *Enteromorpha prolifera*. *Ecotoxicology and Environmental Safety* **164**, 440–447.

Chen, W., Wei, R., Yang, L., Yang, Y., Li, G. & Ni, J. 2019 Characteristics of wood-derived biochars produced at different temperatures before and after deashing: their different potential advantages in environmental applications. *Science of the Total Environment* **651** (Pt 2), 2762–2771.

Deng, H., Yang, L., Tao, G. & Dai, J. 2009 Preparation and characterization of activated carbon from cotton stalk by microwave assisted chemical activation – application in methylene blue adsorption from aqueous solution. *Journal of Hazardous Materials* **166** (2–3), 1514–1521.

Dotto, G. L., Pinto, L. A. A., Hachicha, M. A. & Knani, S. 2015 New physicochemical interpretations for the adsorption of food dyes on chitosan films using statistical physics treatment. *Food Chemistry* **171**, 1–7.

Du, H., Wu, J., Li, H., Zhong, P.-X., Xu, Y.-J., Li, C.-H., Ji, K.-X. & Wang, L.-S. 2013 Polyphenols and triterpenes from *Chaenomeles* fruits: chemical analysis and antioxidant activities assessment. *Food Chemistry* **141** (4), 4260–4268.

Hamauzu, Y., Yasui, H., Inno, T., Kume, C. & Omanyuda, M. 2005 Phenolic profile, antioxidant property, and anti-influenza viral activity of Chinese quince (*Pseudocydonia sinensis* Schneid.), quince (*Cydonia oblonga* Mill.), and apple (*Malus domestica* Mill.) fruits. *Journal of Agricultural and Food Chemistry* **53** (4), 928–934.

Han, L., Qian, L., Liu, R., Chen, M., Yan, J. & Hu, Q. 2017 Lead adsorption by biochar under the elevated competition of cadmium and aluminum. *Scientific Reports* **7** (1), 2264.

Hong, M., Zhang, L., Tan, Z. & Huang, Q. 2019 Effect mechanism of biochar's zeta potential on farmland soil's cadmium immobilization. *Environmental Science and Pollution Research* **26** (19), 19738–19748.

Ippolito, J. A., Strawn, D. G., Scheckel, K. G., Novak, J. M., Ahmedna, M. & Niandou, M. A. S. 2012 Macroscopic and molecular investigations of copper sorption by a steam-activated biochar. *Journal of Environmental Quality* **41** (4), 1150–1156.

Jalayeri, H. & Pepe, F. 2019 Novel and high-performance biochar derived from pistachio green hull biomass: production, characterization, and application to Cu(II) removal from aqueous solutions. *Ecotoxicology and Environmental Safety* **168**, 64–71.

Ji, Z. & Pei, Y. 2019 Competitive adsorption property of multi-metals in static and dynamic process using millet chaff-based biochar. *DWT* **163**, 143–154.

Keiluweit, M., Nico, P. S., Johnson, M. G. & Kleber, M. 2010 Dynamic molecular structure of plant biomass-derived black carbon (biochar). *Environmental Science & Technology* **44** (4), 1247–1253.

Kołodyńska, D., Wnętrzak, R., Leahy, J. J., Hayes, M. H. B., Kwapiński, W. & Hubicki, Z. 2012 Kinetic and adsorptive characterization of biochar in metal ions removal. *Chemical Engineering Journal* **197**, 295–305.

Kumar, U., Maroufi, S., Rajarao, R., Mayyas, M., Mansuri, I., Joshi, R. K. & Sahajwalla, V. 2017 Cleaner production of iron by using waste macadamia biomass as a carbon resource. *Journal of Cleaner Production* **158**, 218–224.

Li, H., Dong, X., da Silva, E. B., de Oliveira, L. M., Chen, Y. & Ma, L. Q. 2017 Mechanisms of metal sorption by biochars: biochar characteristics and modifications. *Chemosphere* **178**, 466–478.

Li, C., Zhang, L., Gao, Y. & Li, A. 2018 Facile synthesis of nano ZnO/ZnS modified biochar by directly pyrolyzing of zinc contaminated corn stover for Pb(II), Cu(II) and Cr(VI) removals. *Waste Management* **79**, 625–637.

Liu, W., Sun, W., Han, Y., Ahmad, M. & Ni, J. 2014 Adsorption of Cu(II) and Cd(II) on titanate nanomaterials synthesized via hydrothermal method under different NaOH concentrations: role of sodium content. *Colloids and Surfaces A: Physicochemical and Engineering Aspects* **452**, 138–147.

Niazi, N. K., Bibi, I., Shahid, M., Ok, Y. S., Shaheen, S. M., Rinklebe, J., Wang, H., Murtaza, B., Islam, E., Farrakh Nawaz, M. & Lüttge, A. 2018 Arsenic removal by Japanese oak wood biochar in aqueous solutions and well water: investigating arsenic fate using integrated spectroscopic and microscopic techniques. *Science of the Total Environment* **621**, 1642–1651.

Novak, J. M., Lima, I., Xing, B., Gaskin, J. W., Steiner, C., Das, K. C., Ahmedna, M., Rehrah, D., Watts, D. W., Busscher, W. J. & Schomberg, H. 2009 Characterization of designer biochar produced at different temperatures and their effects on a loamy sand. *Annals of Environmental Science* **3**, 195–206.

Peng, H., Gao, P., Chu, G., Pan, B., Peng, J. & Xing, B. 2017 Enhanced adsorption of Cu(II) and Cd(II) by phosphoric acid-modified biochars. *Environmental Pollution* **229**, 846–853.

Richard, F. C. & Bourg, A. C. M. 1991 Aqueous geochemistry of chromium: a review. *Water Research* **25** (7), 807–816.

Sellaoui, L., Guedidi, H., Knani, S., Reinert, L., Duclaux, L. & Ben Lamine, A. 2015 Application of statistical physics formalism to the modeling of adsorption isotherms of ibuprofen on activated carbon. *Fluid Phase Equilibria* **387**, 103–110.

Shakya, A. & Agarwal, T. 2019 Removal of Cr(VI) from water using pineapple peel derived biochars: adsorption potential and re-usability assessment. *Journal of Molecular Liquids* **293**, 111497.

Shen, Y., Wang, S., Tzou, Y., Yan, Y. & Kuan, W. 2012 Removal of hexavalent Cr by coconut coir and derived chars – the effect of surface functionality. *Bioresource Technology* **104**, 165–172.

Shen, Z., Hou, D., Jin, F., Shi, J., Fan, X., Tsang, D. C. W. & Alessi, D. S. 2019 Effect of production temperature on lead removal mechanisms by rice straw biochars. *Science of the Total Environment* **655**, 751–758.

Song, J., He, Q., Hu, X., Zhang, W., Wang, C., Chen, R., Wang, H. & Mosa, A. 2019 Highly efficient removal of Cr(VI) and Cu(II) by biochar derived from *Artemisia argyi* stem. *Environmental Science and Pollution Research* **26** (13), 13221–13234.

Tong, X.-j., Li, J.-y., Yuan, J.-h. & Xu, R.-k. 2011 Adsorption of Cu(II) by biochars generated from three crop straws. *Chemical Engineering Journal* **172** (2–3), 828–834.

Tytłak, A., Oleszczuk, P. & Dobrowolski, R. 2015 Sorption and desorption of Cr(VI) ions from water by biochars in different environmental conditions. *Environmental Science and Pollution Research* **22** (8), 5985–5994.

Uchimiya, M., Wartelle, L. H., Klasson, K. T., Fortier, C. A. & Lima, I. M. 2011 Influence of pyrolysis temperature on biochar property and function as a heavy metal sorbent in soil. *Journal of Agricultural and Food Chemistry* **59** (6), 2501–2510.

Venugopal, V. & Mohanty, K. 2011 Biosorptive uptake of Cr(VI) from aqueous solutions by *Parthenium hysterophorus* weed: equilibrium, kinetics and thermodynamic studies. *Chemical Engineering Journal* **174** (1), 151–158.

Wang, J. & Wang, S. 2019 Preparation, modification and environmental application of biochar: a review. *Journal of Cleaner Production* **227**, 1002–1022.

Wang, H., Gao, B., Wang, S., Fang, J., Xue, Y. & Yang, K. 2015 Removal of Pb(II), Cu(II), and Cd(II) from aqueous solutions by biochar derived from $KMnO_4$ treated hickory wood. *Bioresource Technology* **197**, 356–362.

Wang, L., Liu, H.-M., Xie, A.-J., Wang, X.-D., Zhu, C.-Y. & Qin, G.-Y. 2018 Chinese quince (*Chaenomeles sinensis*) seed gum: structural characterization. *Food Hydrocolloids* **75**, 237–245.

Wei, J., Tu, C., Yuan, G., Liu, Y., Bi, D., Xiao, L., Lu, J., Theng, B. K. G., Wang, H., Zhang, L. & Zhang, X. 2019a Assessing the effect of pyrolysis temperature on the molecular properties and copper sorption capacity of a halophyte biochar. *Environmental Pollution* **251**, 56–65.

Wei, S., Zhu, M., Fan, X., Song, J., Peng, P., Li, K., Jia, W. & Song, H. 2019b Influence of pyrolysis temperature and feedstock on carbon fractions of biochar produced from pyrolysis of rice straw, pine wood, pig manure and sewage sludge. *Chemosphere* **218**, 624–631.

Yang, Y., Zhang, W., Qiu, H., Tsang, D. C. W., Morel, J.-L. & Qiu, R. 2016 Effect of coexisting Al(III) ions on Pb(II) sorption on biochars: role of pH buffer and competition. *Chemosphere* **161**, 438–445.

Zhang, L., Cheng, Y.-X., Liu, A.-L., Wang, H.-D., Wang, Y.-L. & Du, G.-H. 2010 Antioxidant, anti-inflammatory and anti-influenza properties of components from *Chaenomeles speciosa*. *Molecules* **15** (11), 8507–8517.

Zhang, W., Deng, Q., He, Q., Song, J., Zhang, S., Wang, H., Zhou, J. & Zhang, H. 2018a A facile synthesis of core-shell/bead-like poly(vinyl alcohol)/alginate@PAM with good adsorption capacity, high adaptability and stability towards Cu(II) removal. *Chemical Engineering Journal* **351**, 462–472.

Zhang, W., Zhang, S., Wang, J., Wang, M., He, Q., Song, J., Wang, H. & Zhou, J. 2018b Hybrid functionalized chitosan-Al_2O_3@SiO_2 composite for enhanced Cr(VI) adsorption. *Chemosphere* **203**, 188–198.

Zhang, P., Li, Y., Cao, Y. & Han, L. 2019a Characteristics of tetracycline adsorption by cow manure biochar prepared at different pyrolysis temperatures. *Bioresource Technology* **285**, 121348.

Zhang, W., Wang, H., Hu, X., Feng, H., Xiong, W., Guo, W., Zhou, J., Mosa, A. & Peng, Y. 2019b Multicavity triethylenetetramine-chitosan/alginate composite beads for enhanced Cr(VI) removal. *Journal of Cleaner Production* **231**, 733–745.

Zhao, S., Ta, N. & Wang, X. 2017 Effect of temperature on the structural and physicochemical properties of biochar with apple tree branches as feedstock material. *Energies* **10** (9), 1293.

Zhao, B., O'Connor, D., Zhang, J., Peng, T., Shen, Z., Tsang, D. C. W. & Hou, D. 2018 Effect of pyrolysis temperature, heating rate, and residence time on rapeseed stem derived biochar. *Journal of Cleaner Production* **174**, 977–987.

Zhou, L., Liu, Y., Liu, S., Yin, Y., Zeng, G., Tan, X., Hu, X., Hu, X., Jiang, L., Ding, Y., Liu, S. & Huang, X. 2016 Investigation of the adsorption-reduction mechanisms of hexavalent chromium by ramie biochars of different pyrolytic temperatures. *Bioresource Technology* **218**, 351–359.

First received 15 October 2019; accepted in revised form 21 January 2020. Available online 29 January 2020